Infrared Lock-in Thermography Tests with Optical Feedback

António Ramos Silva[1], Mário Vaz[2], Sofia Leite[3], Joaquim Mendes[4]

[1]Faculty of Engineering, University of Porto, Rua Dr. Roberto Frias, 4200-465 Porto, Portugal; INEGI - Institute of Science and Innovation in Mechanical and Industrial Engineering, Faculty of Engineering campus, Rua Dr. Roberto Frias, 4200-465 Porto, Portugal (ars@fe.up.pt) ORCID 0000-0002-4146-6224; [2]Faculty of Engineering, University of Porto, Rua Dr. Roberto Frias, 4200-465 Porto, Portugal; INEGI - Institute of Science and Innovation in Mechanical and Industrial Engineering, Faculty of Engineering campus, Rua Dr. Roberto Frias, 4200-465 Porto, Portugal (gmvaz@fe.up.pt) ORCID 0000-0002-6347-9608; [3]Faculty of Engineering, University of Porto, Rua Dr. Roberto Frias, 4200-465 Porto, Portugal; CINTESIS-Center for Health Technology and Services Research, Faculty of Medicine, University of Porto, 4200-450 Porto, Portugal (sofiarsleite@gmail.com) ORCID 0000-0003-3999-2492; [4]Faculty of Engineering, University of Porto, Rua Dr. Roberto Frias, 4200-465 Porto, Portugal (jgabriel@fe.up.pt) ORCID 0000-0003-4254-1879

Abstract

The detection of defects in structural elements can be performed by lock-in infrared thermography using a period light stimulation. However, the results are highly dependent on the accuracy of the stimulation source and its dynamic response. This work aimed to evaluate the quality of a light source as a thermal stimulation and its influence on the quality of the lock-in tests performed in PMMA samples. For this purpose, it was developed an enhanced technique, feedback lock-in thermal testing (FLTT), which uses a light sensor to measure the real light stimulation. With this solution, it was possible to improve the signal-to-noise ratio of the amplitude and phase images by approximately 2.5 times. Although only one commercial stimulation source has been tested, others may present similar behavior. Thus, this technique may be considered for lock-in systems using light stimulation, as the increment of the cost is rather small.

Author Keywords. Thermography. Lock-in. Non-destructive Testing. PMMA Defects. Light Stimulation.

Type: Research Article

1. Introduction

The transportation industry involves millions of vehicles worldwide, which requires constant structural optimization to improve safety and reduce weight. Thus, the demand for better-performing materials, namely composite materials, has gained a high interest. They can provide an excellent trade-off between weight and mechanical properties, which are difficult to match with other materials. Among the diversity of composite materials, Carbon and Glass Fiber Reinforced Polymers (CFRP, GFRP) are widely used, being the first the most suitable for demanding applications (Holmes 2013). For safety reasons, it is mandatory to perform regular check-ups and maintenance operations which can range from simple routine inspections to deeper and more detailed operations, requiring top-of-the-line equipment.

Currently, Non-Destructive Testing (NDT) is often the best manner of assessing the integrity of a component. NDT allows the evaluation of the component properties (density, stiffness, thermal conductivity) in search of discontinuities that are connected to structural defects (Park et al. 2014; Mix 2005). Despite NDT techniques, like ultrasounds, being very precise, they

usually take a long time to scan even a small area. However, it is possible to increase the evaluation speed by using field image techniques, which have the advantage of scanning large areas but tend to lose sensibility, especially when evaluating thicker components. The most used testing techniques are radiographic, dye inspections, holographic interferometry, shearography, and thermography. Among them, the last one - Infrared Thermal Testing - has been showing very good and consistent results, with the advantage of not using ionizing radiation and being safe for humans (Keo et al. 2014; Liu et al. 2014; Maldague 2012; Renshaw et al. 2011; Keo et al. 2015). Additionally, infrared thermography can be combined with different stimulation sources like ultrasounds, microwaves, vibrations, visible light, etc. This stimulation provokes a change in the object's temperature, which improves the capability of Infrared Thermography to detect and characterize a defect (Mountain and Webber 1979; Plum and Ummenhofer 2009; Keo et al. 2013). Over the last decades, several numeric models have been developed, allowing to estimate the temperature with great sensibility near millikelvin (Breitenstein, Warta, and Langenkamp 2010). The stimulation can be modulated as a transient stimulation (Pulse) or periodic, like a sine waveform, with the last providing the observation of deeper defects (Giorleo, Meola, and Squillace 2000; Avdelidis, Hawtin, and Almond 2003; Chatterjee et al. 2011). This technique is denominated Lock-in Thermal Testing (LTT).

The analysis performed with LTT is like the one performed in electric circuits, from which this technique originated. The purpose behind the use of cyclic stimulation is to evaluate its dynamic response, thus increasing the resolution and sensibility of the measurement. During an LTT, the temperature images recorded are analyzed afterward. The evolution of each pixel (temperature wave) is compared to the reference and calculated the amplitude and phase differences images. This process assumes that the reference signal and real stimulus are similar, which is not always true.

This work intends to show that it is possible to improve the defect detection sensibility of a commercial system by measuring the real light stimulation and then correcting the reference to the Lock-in.

The following section presents considerations about the amplitude and phase calculus. The third section presents the laboratory setup and stimulus characterization. The fourth section presents an enhanced LTT technique called Feedback LTT (FLTT), which corrects the stimulation curve. The fifth and sixth sections analyzed, compared, and discussed the results obtained with the LTT and FLTT.

2. System Analysis

2.1. Stimulus characterization

The main goal of these tests was to characterize the stimulus produced by the halogen lamps (HEDLER, Berlin, Germany) having a maximum power of 2500 W, connected to a power unit, the powerbox model from Automation & Technology. This source has the advantage of being contactless; however, it has limitations regarding following high frequencies. The system was controlled by the software IRNDT version 1.7 (Bad Oldesloe, Germany), and the images were processed and analyzed using MATLAB® 2019 (Mathworks, Natick, MA, USA).

A light-dependent resistor (LDR) photocell from CdS model GL55 was used as stimulation light feedback. This sensor output resistance ranges from 10Ω to 1MΩ, corresponding to the maximum and minimum light, respectively, with a linear variation given by the respective signal conditioning. On top of the light entrance, a filter was placed to diminish the amount of light reaching the sensor, thus preventing saturation, as recommended by the sensor

manufacturer. The sensor waveband ranges approximately from 400 to 800 nm, which corresponds to the visible spectrum. According to the lamps' manufacturer, the glass protecting the halogen lamps blocks most of the radiation in the ultraviolet and infrared wavebands, freeing the visible spectrum, which is measured by the sensor.

The measurements were performed using a data acquisition system from National Instruments™ (TX, USA), board model NI USB-6251 (Figure 1), which is connected to the light sensor unit, the Power box (reference signal), and to the feedback of the reference it-self (just to warranty the time clock is the same for all input signals).

During the characterization and the thermal tests, the stimulation source (halogen lamps), thermal camera, lightbox sensor, and sample were held in place by a structure built using Bosch® aluminum profiles. The sensor was positioned position close to the sample and had the same orientation.
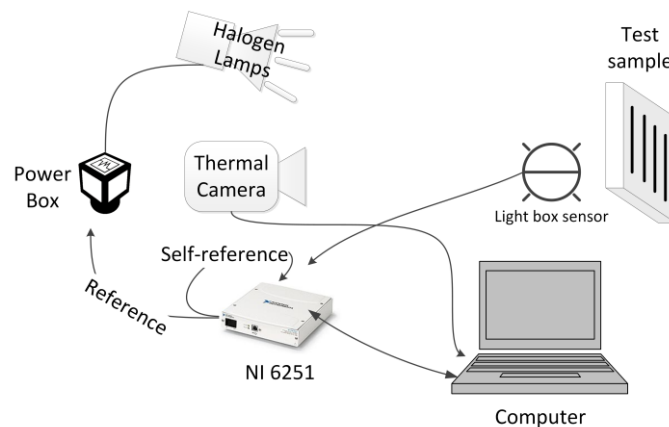

Figure 1: Schematic of the setup used in the evaluation of the light source

To perform the stimulus characterization, a custom application written in LabVIEW™ was developed, which allows the creation of a sweep sine waveform composed of 50 cycles, with a period between 20s to 0.5 s, and a range from 0 to 10 V. The reference signal started with a phase of - 90 ° (co-sin wave type), thus starting with minimum value and allowing a continuous function between cycles.

The NI board generates the electrical reference signal (1000 samples per second), and the power box amplifies it. For the testing conditions, the light sensor unit output ranged from 1.2 to 4.5 V for the maximum and minimum light, respectively. The reference and light sensor output were normalized so that they could be easily compared. For this purpose, were considered the baseline values (before the first stimulation) and the maximum value when the reference was set to 100% for 10 seconds.

Two evaluations were performed, one with a square and the other with a sinusoidal wave stimulation signal. The optical response to a square wave reference, Figure 2, shows a steady-state error. Also, when the reference changed from zero to one, the light response presents a delay of approximately 0.5 s, while when changed from one to zero, the light responds slower, being necessary approximately two seconds to reach the steady-state value. This behavior indicates a different settling time for a positive and negative transition. The usage of a Halogen lamp, which will heat when an electrical current flows through it and thus change the filament resistivity, explains various points, namely: i) since the normalization was performed with the first positive transition when the filament was at its coldest temperature, the light sensor signal never reaches again the value of 1, ii) after applying a small amount of light, its

temperature increases along with its resistance thus, decreasing the electrical current and the generated light, resulting in steady-state errors (Figure 2).
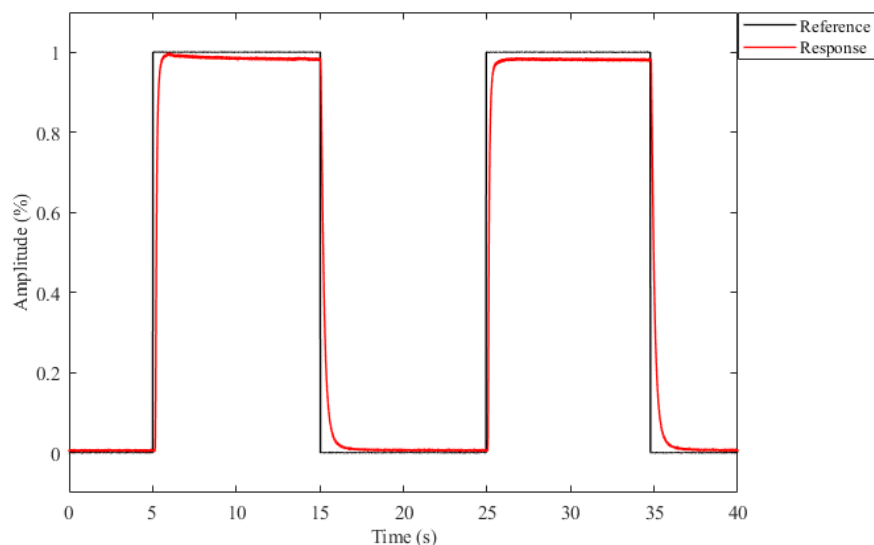

Figure 2: Light response to slow square wave stimulation

Figure 3 and Figure 4 show the difficulty of the system in responding to a sinusoidal wave, either with low or high frequencies. When using a sinusoidal reference with low frequency (Figure 3), the resulting stimulation presents some similarities to a square wave. This shows a lack of proportionality between the reference signal and the produced light stimulation. Even if the electrical power created by the reference may be proportional to the reference signal, the light signal is not. This may be due to the variation in the electrical resistance of the lamp, as mentioned above.
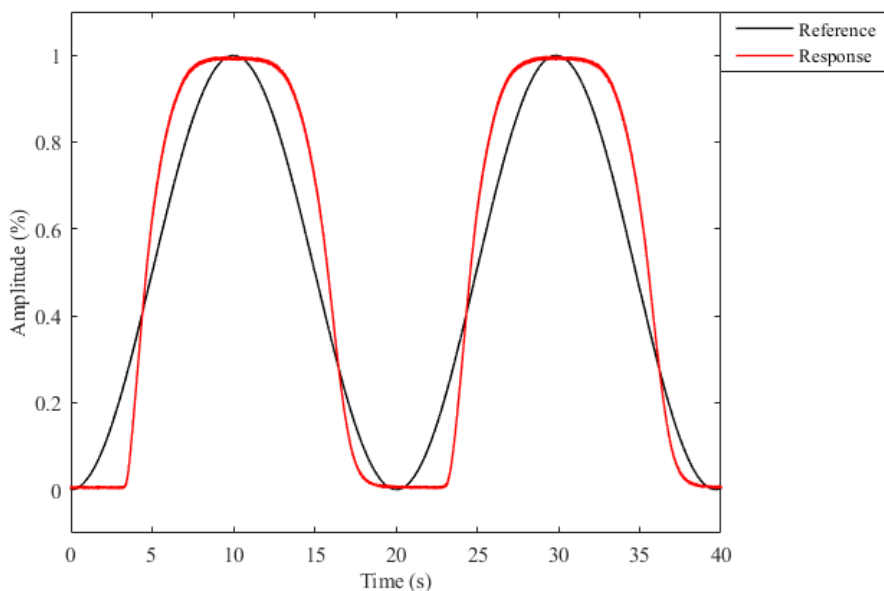

Figure 3: Light response of the halogen lamp to slow sinusoidal stimulations

Figure 4 shows the system's difficulty in following frequencies higher than 1 Hz. As expected, with the increase of the frequency, the amplitude decreases. In addition, the delay between the light reference and response is higher in the lower half of the curve when rising and in the higher half when falling. The overall behavior of the stimulation is poor.
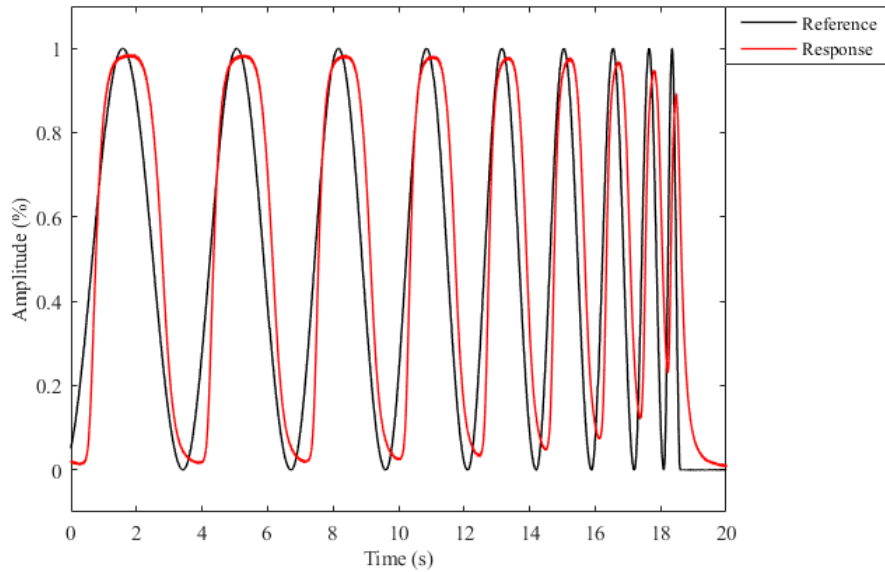
Figure 4: Light response to fast sinusoidal stimulation (frequencies 0.25-2 Hz)

2.2. Amplitude and phase

The traditional light stimulation in LTT uses an open-loop control system (no feedback). Therefore, there is no assurance that the sample receives a sinusoid stimulation when undergoing an LTT, which has implications for the results.

To evaluate the dynamic response of the system, it was performed a sinusoidal wave sweep between 0.25 and 2 Hz (Figure 4), with a constant amplitude of 1 (normalized). The system response (Y), Equation (1), is given by the product of the stimulation by the system function (Goldman 2007).

$$Y(j\omega) = H(j\omega) \times X(j\omega) \tag{1}$$

Where:

$Y(j\omega)$ – system output (temperature measurement)

$X(j\omega)$ – system input (stimulation)

$H(j\omega)$ – real system (sample)

Thus, the system amplitude (A) and phase response (Φ) is then calculated using Equation (2):

$$\begin{aligned} A(\omega) &= |H(j\omega)| \\ \Phi(j\omega) &= \angle\, H(j\omega) \end{aligned} \tag{2}$$

With each being obtained through Equation (3).

$$\begin{aligned} A(\omega) &= \frac{|Y(j\omega)|}{|X(j\omega)|} \\ \Phi(\omega) &= \angle\, Y(j\omega) - \angle\, X(j\omega) \end{aligned} \tag{3}$$

By applying a waveform with multiple frequencies, it results in a system response also with multiple amplitudes and phase responses, one for each of the stimulation frequencies. These results are usually presented in a Bode plot. However, if the stimulation has a single frequency (like in the case of the LTT), the response will be predominantly in that same frequency (Ogata 2009). Thus, the amplitude and phase response will have a single value for each. If one normalized the reference signal, the amplitude response could be expressed in temperature (Kelvin, for example).

There are several methods to calculate the frequency response based on experimental data (Quek et al. 2005); most of them were developed for electrical circuits, sound processing, and closed-loop control systems. However, in these situations, the stimulation curve is always

measured, contrary to the LTT procedure. Consequently, if the stimulation is not exactly equal to the theoretical wave, the results are incorrect.

3. Feedback Lock-in Thermal Tests

3.1. Setup and settings

After the characterization of the light stimulation, this section evaluates its impact in the Infra-Red Non-Destructive Test (IRNDT). This section presents the samples, setup, results, and analysis from a common Lock-in Thermal Test (LTT) and the enhanced technique feedback lock-in thermal test (FLTT). The goal of these tests was to quantify the influence of the stimulation curve in an LTT.

The following tests used two samples made from PMMA with 4 machined slots (Figure 5). The samples are 210 by 160 mm in size (width and height), with slots of 5 mm (sample 1) and 10 mm (sample 2) width and 4 different depths. Due to the similarity of the results obtained for both samples, only the results for the sample with slots of 10 mm are presented. PMMA ensures the samples are isotropic and their thermal properties are similar to CFRP or GFRP.
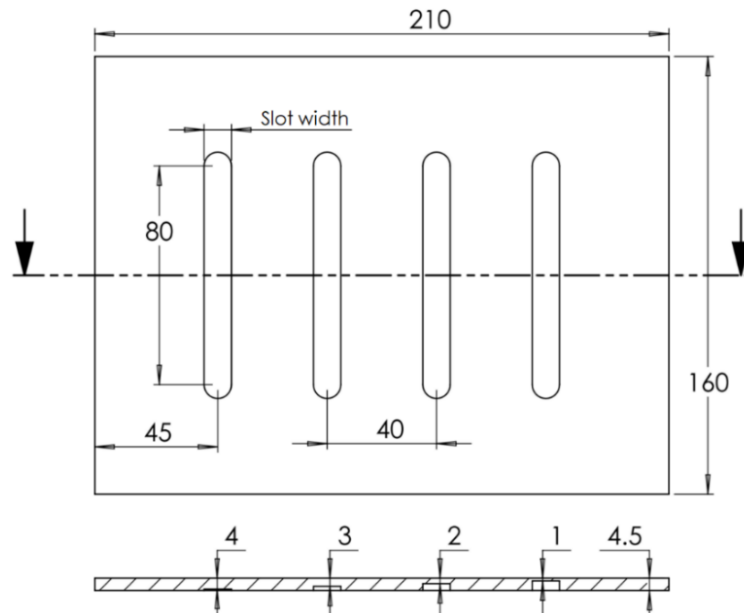

Figure 5: Overall dimensions of the samples

Figure 6 presents the experimental setup. The sample is placed in a vertical position, held by two pins to prevent heat conduction, and better simulate real maintenance operations. The thermal camera was placed perpendicularly at approximately 1 meter from the sample. The stimulation was right above the camera (approximately 0.8 m), in a reflective mode positioning. A wooden plat placed behind the sample provides a uniform background.

Each test consisted in the application of 15 cycles, being recorded 4500 images (300 images per cycle). The amplitude and phase images are created by comparing each pixel with the reference. The phase images may provide a deeper and more sensitive analysis than the amplitude images (Silva et al. 2019). However, it may suffer from blind frequencies. If the stimulation frequency is such that the defect response is in phase with the stimulation, the defect becomes invisible, making the test blind for that defect (Chatterjee and Tuli 2013). The phase images were used to detect the defects and compare the two techniques.
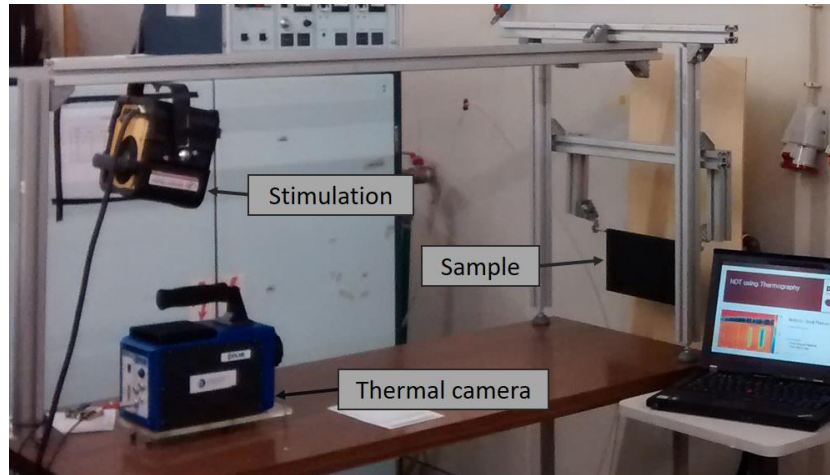
Figure 6: Experimental setup

The software used in this work supports the calculations according to the Thermal Signal Reconstruction (TSR) method. The images were obtained using two different processing methods, harmonic approximation and single-frequency Discrete Fourier Transform (DFT). When performing a numerical comparison between both methodologies, they produced identical images (Silva et al. 2019). Thus, the single-frequency DFT was selected. The images were exported in raw data, the only available option, and each image was then analyzed in MATLAB®. The first step of the analysis was to crop the images to remove the background, as illustrated in Figure 7. To perform a deeper and more detailed analysis, in each image, a single average horizontal profile was produced by averaging 30 horizontal cross-section profiles, white rectangle (Figure 7). The averaged process acted as a filter for the thermal profiles, reducing the noise. In an FLTT, the temperature data is equal to the LTT. The difference is in the reference signal. The LTT uses a perfect sinusoid, while the FLTT uses real data from the light sensor unit.
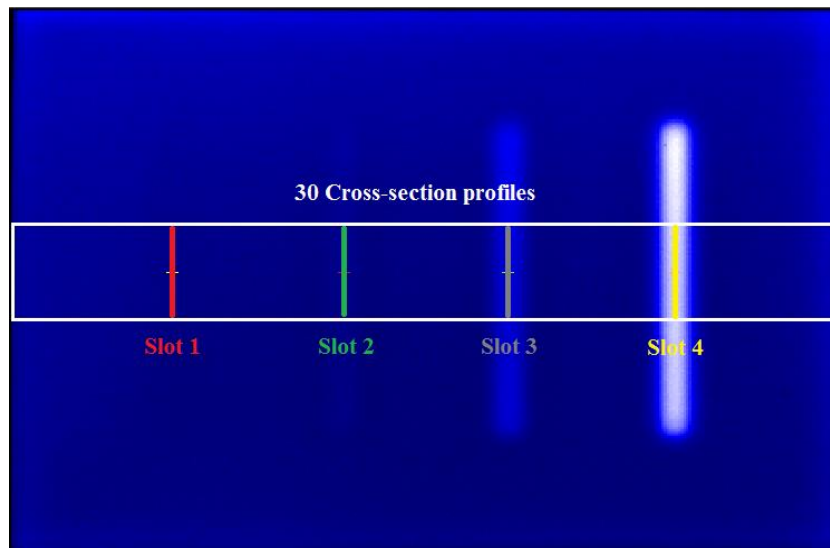

Figure 7: Image after processing with 30 horizontal profiles (white rectangle) used to obtain the average temperature profiles

3.2. Test results and analyses

The most important aspect when comparing the images from the two LTT techniques is the ratio between the thermal response in the slots and the magnitude of the noise existing in the image. This can be defined as the signal-to-noise ratio (SNR), Equation (4). Where $\overline{x}_s$, $\overline{x}_{sa}$, and $x_{i(sa)}$ are calculated for the amplitude and the phase.

$$SNR = \frac{\overline{x}_s - \overline{x}_{sa}}{\sqrt{\dfrac{\sum\left(x_{i(sa)} - \overline{x}_{sa}\right)^2}{N}}}$$

(4)

Where:

$\overline{x}_s$ – slot average value from the amplitude or phase images;

$\overline{x}_{sa}$ – sound area average value from the amplitude or phase images;

$x_{i(sa)}$ – value at the slot location from the amplitude or phase images, $1 \leq i \leq 30$

N – number of profiles (30).

To compare the two techniques, the average and standard deviation of the SNR were calculated in five areas. These are located at the 4 corners of the cropped images and one at its center, with a size of 10 pixels in width and 30 in height. The standard deviation obtained from the LTT with 30-second stimulation served as a reference. Finally, the images were scaled to a standard deviation of one. The results from three responses, corresponding to the stimulation periods of 10, 20, and 30 are represented in Figure 8. The amplitude data is presented as ADC readings, the raw value of the analog-to-digital converter (ADC) of the thermal camera, before being converted to temperature. This is due to a limitation of the software, which does not allow to export temperature data, but only raw data.
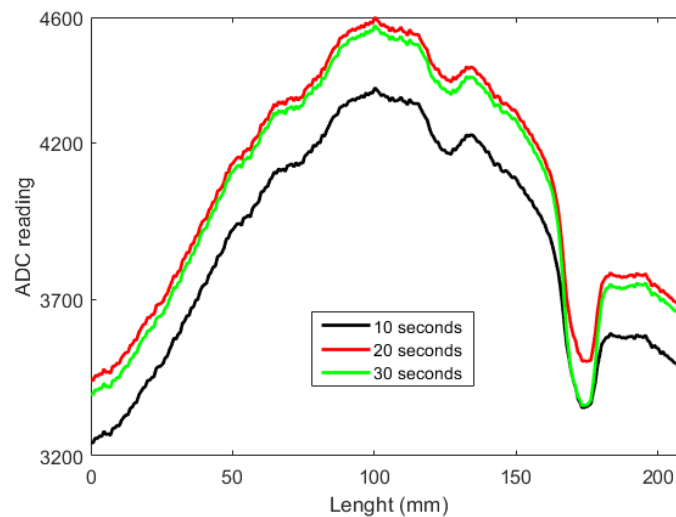

Figure 8: ADC readings of the thermal camera for the lock-in tests with 10, 20, and 30 s periods

Another important aspect was the high amplitude response in the middle of the amplitude images (bell shape curves). This is a consequence of the reflection from the light stimulation. Using a low-cut filter, this artifact was almost cleared out. All amplitude images passed through this process, resulting in the average cross-section profiles representing it (Figure 9). This image corresponds to the amplitude obtained with LTT (20 seconds) and feedback lock-in thermal test FLTT (10-, 20-, and 30-second cycle periods).

Comparing the thermal response of the FLTT with LTT for a 20-second stimulation, a higher sensitivity for all three FLTT was found, mainly at slot 4. In the LTT, slot 3 is slightly visible, while in the FLTT profiles, this leaves no margin for doubt. Slot 2 is only visible with the FLTT. Thus, the FLTT not only gives a higher signal-to-noise ratio in the deeper defects but is also able to detect defects not visible with the LTT.
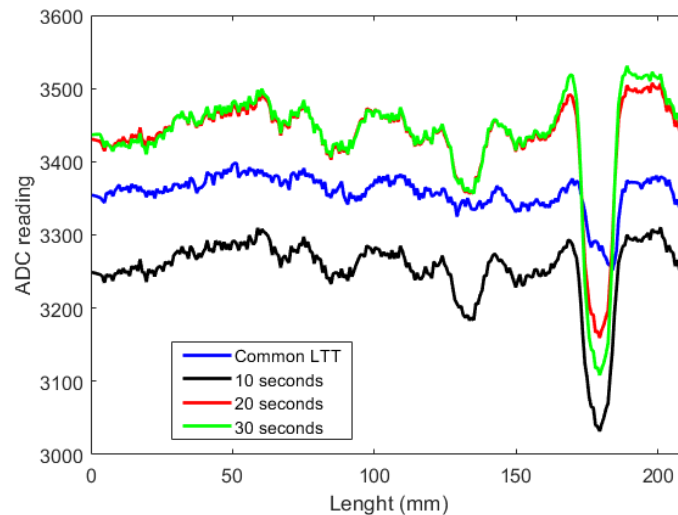
Figure 9: Averaged cross-section profiles for LTT and FLTT

4. Discussion

During the last decades, several groups have been developing the LTT methodology, correlating certain thermal patterns with the defect geometry and comparing it with other techniques.

In lock-in tests, the assumption that the stimulation waveform is accurate is common; however, this is not true. The usage of a light sensor to measure the stimulation revealed that the real waveform was considerably different from the assumed (and desired perfect sinusoid). The usage of a square reference reveals a delay of 0.5 s in low to high transition and 2 s in the high-to-low falling, as observed in Figure 2.

The stimulation using a sinusoidal reference with a period of 20 seconds is far more resembling a square wave than initially expected. This indicated a non-proportionality between the desired waveform and the produced light stimulation. However, a stimulation that resembles a sinusoidal wave was obtained with a cycle period of about 2 seconds, which is not a typical testing period, particularly in the analyses of polymeric or composite materials.

In this work, the harmonic approximation and single DFT methods were used to approximate the temperature curves. These give similar results as presented in other works (Silva et al. 2019). Thus, the results obtained using the light feedback signal should be equal when using other processing techniques.

Despite having calibrated the camera according to Flir recommendations, it was observed a small offset at the center of the temperature images, which is due to some reflection coming. In the amplitude and particular in phase images, this effect is less visible. However, this error was removed by applying a low-pass filter, as seen in Figure 9.

When analyzing an IRNDT image, it is important to comprehend the causes of the different thermal responses (Figure 8 and Figure 9). The sound areas are thicker than the slots and therefore present a higher thermal resistance. Thus, the profiles for longer stimulations present higher slot detectability, as observed in Figure 8 and Figure 9.

The ability to distinguish the defect from the sound area is called defect detectability. The ratio between the thermal response in the slots and the magnitude of the noise existing in the image is called the signal-to-noise ratio (SNR). The images from the LTT and FLTT were normalized, so the noise amplitude of the five areas shows an equal level of noise in all images. This way, a direct comparison of the signals at the slot locations is possible.

A comparison between 20 seconds LTT (reference test) and FLTT with cycle periods of 10, 20, and 30 seconds was conducted. In all the analyses performed with the two samples, the detectability is higher when using the light feedback (FLTT). The smallest cycle period, 10 seconds, also delivered a smaller amount of energy which, combined with the small thermal conductivity of the PMMA, resulted in low thermal differences, as expected (Junyan, Liqiang, and Yang 2013). For this technique, the stimulations of 20 and 30 seconds resulted in similar amplitude average profiles.

From Figure 9, two observations relating to the FLTT can be made: its detectability increases when compared with the LTT, and the signal-to-noise ratio is greater. FLTT was able to detect the smaller thermal differences, and thus all the slots, improving the detectability by a magnitude of 2.5. In other words, the FLTT technique is 2.5 times more sensitive.

5. Conclusions

The assumption that the light stimulation applied to the Lock-in Thermal Test is a perfect sinusoidal can result in large errors and diminish the test sensitivity to certain defects. The performance of the power controller used with these optical devices plays an important role in the performance of the LTT equipment. Additionally, the lamp's filament warming naturally introduces a delay in the stimulation.

Usually, the phase images are more sensible than the amplitude. However, they are also more sensitive to the existence of noise in the temperature data. Using the real stimulation curve helps to overcome this problem, increases the similarities between the two curves, and reduces the noise in the amplitude and phase images. The result is an increase in the sensitivity of the LTT, well visible when comparing the LTT and FLTT average profiles.

The new approach proposed, which uses light feedback, increases the defect detectability and the signal-to-noise ratio of the LTT. For the current equipment, this improvement was approximately 2.5 times. Therefore, it is possible to use shorter cycle periods, and thus the test duration can be shortened.

Different equipment can produce stimulation waves that differ from the results of these tests. Thus, these results can vary for other test equipment. However, using a light feedback sensor, it is possible to reduce the errors, increase sensitivity and can help to standardize the LTT and its results.

References

Avdelidis, N. P., B. C. Hawtin, and D. P. Almond. 2003. "Transient thermography in the assessment of defects of aircraft composites". *NDT & E International* 36, no. 6: 433-39. https://doi.org/10.1016/S0963-8695(03)00052-5.

Breitenstein, O., W. Warta, and M. Langenkamp. 2010. *Lock-in thermography: Basics and use for evaluating electronic devices and materials*. Vol. 10. https://doi.org/10.1007/978-3-642-02417-7.

Chatterjee, K., and S. Tuli. 2013. "Prediction of blind frequency in lock-in thermography using electro-thermal model based numerical simulation". *Journal of Applied Physics* 114, no. 17: Article number 174905. https://doi.org/10.1063/1.4828480.

Chatterjee, K., S. Tuli, S. G. Pickering, and D. P. Almond. 2011. "A comparison of the pulsed, lock-in and frequency modulated thermography non-destructive evaluation techniques". *NDT & E International* 44, no. 7: 655-67. https://doi.org/10.1016/j.ndteint.2011.06.008.

Giorleo, G., C. Meola, and A. Squillace. 2000. "Analysis of defective carbon-epoxy by means of lock-in thermography". *Research in Nondestructive Evaluation* 12, no. 4: 241-50. https://doi.org/10.1080/09349840009409663.

Goldman, S. 2007. *Phase-locked Loop Engineering Handbook for Integrated Circuits*. Artech House.

Holmes, M. 2013. "Carbon fibre reinforced plastics market continues growth path". *Reinforced Plastics* 57, no. 6: 24-29. https://doi.org/10.1016/S0034-3617(13)70186-3.

Junyan, L., L. Liqiang, and W. Yang. 2013. "Experimental study on active infrared thermography as a NDI tool for carbon-carbon composites". *Composites Part B: Engineering* 45, no. 1: 138-47. https://doi.org/10.1016/j.compositesb.2012.09.006.

Keo, S. A., D. Defer, F. Breaban, and F. Brachelet. 2013. "Comparison between microwave infrared thermography and CO2 laser infrared thermography in defect detection in applications with CFRP". *Materials Sciences and Applications* 4: 600-05. https://doi.org/10.4236/msa.2013.410074.

Keo, S. A., F. Brachelet, F. Breaban, and D. Defer. 2014. "Steel detection in reinforced concrete wall by microwave infrared thermography". *NDT & E International* 62: 172-77. https://doi.org/10.1016/j.ndteint.2013.12.002.

———. 2015. "Defect detection in CFRP by infrared thermography with CO2 Laser excitation compared to conventional lock-in infrared thermography". *Composites Part B: Engineering* 69: 1-5. https://doi.org/10.1016/j.compositesb.2014.09.018.

Liu, J., G. Y. Tian, B. Gao, W. Ren, and J. S. Meng. 2014. "Investigation of thermal imaging sampling frequency for eddy current pulsed thermography". *NDT & E International* 62: 85-92. https://doi.org/10.1016/j.ndteint.2013.11.009.

Maldague, X. P. V. 2012. *Non-destructive Evaluation of Materials by Infrared Thermography*. Springer Science & Business Media.

Mix, P. E. 2005. *Introduction to Non-destructive Testing: A Training Guide*. 2nd ed.: John Wiley & Sons, Inc. https://doi.org/10.1002/0471719145.

Mountain, D. S., and J. M. B. Webber. 1979. "Stress Pattern Analysis By Thermal Emission (SPATE)". In *Proceedings of SPIE - The International Society for Optical Engineering*, 189-96. https://doi.org/10.1117/12.965516.

Ogata, K. 2009. *Modern control engineering*. 5th ed. Boston: Pearson.

Park, H., M. Choi, J. Park, and W. Kim. 2014. "A study on detection of micro-cracks in the dissimilar metal weld through ultrasound infrared thermography". *Infrared Physics and Technology* 62: 124-31. https://doi.org/10.1016/j.infrared.2013.10.006.

Plum, R., and T. Ummenhofer. 2009. "Ultrasound excited thermography of thickwalled steel load bearing members". *Quantitative InfraRed Thermography Journal* 6, no. 1: 79-100. https://doi.org/10.3166/qirt.6.79-100.

Quek, S., D. Almond, L. Nelson, and T. Barden. 2005. "A novel and robust thermal wave signal reconstruction technique for defect detection in lock-in thermography". *Measurement Science and Technology* 16, no. 5: 1223-33. https://doi.org/10.1088/0957-0233/16/5/024.

Renshaw, J., J. C. Chen, S. D. Holland, and R. Bruce Thompson. 2011. "The sources of heat generation in vibrothermography". *NDT & E International* 44, no. 8: 736-39. https://doi.org/10.1016/j.ndteint.2011.07.012.

Silva, António Ramos, M. Vaz, S. R. Leite, and J. Mendes. 2019. "Non-destructive infrared lock-in thermal tests: Update on the current defect detectability". *Russian Journal of Nondestructive Testing* 55, no. 10: 772-84. https://doi.org/10.1134/S1061830919100097.